

Triangular body-cover model of the vocal folds with coordinated activation of the five intrinsic laryngeal muscles

Gabriel A. Alzamendi,^{1, a)} Sean D. Peterson,^{2, b)} Byron D. Erath,^{3, c)} Robert E. Hillman,^{4, d)} and Matías Zañartu^{5, e)}

¹⁾*Institute for Research and Development on Bioengineering and Bioinformatics (IBB), CONICET-UNER, Oro Verde, Entre Ríos 3100, Argentina^{f)}*

²⁾*Mechanical and Mechatronics Engineering, University of Waterloo, Waterloo, Ontario N2L 3G1, Canada*

³⁾*Department of Mechanical and Aeronautical Engineering, Clarkson University, Potsdam, New York 13699, USA*

⁴⁾*Center for Laryngeal Surgery and Voice Rehabilitation, Massachusetts General Hospital, Boston, Massachusetts 02114, USA^{g)}*

⁵⁾*Department of Electronic Engineering, Universidad Técnica Federico Santa María, Valparaíso 2390123, Chile*

(Dated: 25 November 2021)

Poor laryngeal muscle coordination that results in abnormal glottal posturing is 1
 believed to be a primary etiologic factor in common voice disorders such as non- 2
 phonotraumatic vocal hyperfunction. Abnormal activity of antagonistic laryngeal 3
 muscles is hypothesized to play a key role in the alteration of normal vocal fold 4
 biomechanics that results in the dysphonia associated with such disorders. Current 5
 low-order models of the vocal folds are unsatisfactory to test this hypothesis since 6
 they do not capture the co-contraction of antagonist laryngeal muscle pairs. To ad- 7
 dress this limitation, a self-sustained triangular body-cover model with full intrinsic 8
 muscle control is introduced. The proposed scheme shows good agreement with prior 9
 studies using finite element models, excised larynges, and clinical studies in sustained 10
 and time-varying vocal gestures. Simulations of vocal fold posturing obtained with 11
 distinct antagonistic muscle activation yield clear differences in kinematic, aerody- 12
 namic and acoustic measures. The proposed tool is deemed sufficiently accurate and 13
 flexible for future comprehensive investigations of non-phonotraumatic vocal hyper- 14
 function and other laryngeal motor control disorders. 15

a) galzamendi@ingenieria.uner.edu.ar

b) peterston@uwaterloo.ca

c) berath@clarkson.edu

d) hillman.robert@mgh.harvard.edu

e) matias.zanartu@usm.cl

f) Also at: Facultad de Ingeniería, Universidad Nacional de Entre Ríos, Oro Verde, Entre Ríos 3100, Argentina.

g) Also at: Department of Surgery, Massachusetts General Hospital–Harvard Medical School, Boston, MA02115, USA.

I. INTRODUCTION

Non-phonotraumatic vocal hyperfunction (NPVH) is a common voice disorder associated with excessive and poorly regulated activity of the intrinsic and extrinsic laryngeal muscles (Hillman *et al.*, 2020), causing a range of different types of disordered voice quality (Van Stan *et al.*, 2021) but without trauma to the vocal fold (VF) tissue. A common manifestation of NPVH during phonation is high levels of stiffness and tension in the VFs accompanied by incomplete glottal closure causing the voice to be rough, strained, and breathy with increased subglottal pressure and slightly higher, less periodic, and less variable pitch (Espinoza *et al.*, 2020, 2017; Hillman *et al.*, 2020; Van Stan *et al.*, 2021). Very little is known about the specific physical mechanisms that underlie this or other manifestations of NPVH. However, the apparent increase in muscle activity and vocal fold stiffness, abducted glottal configuration, and relatively restricted pitch variability suggest that poor coordination of antagonist laryngeal muscle pairs plays a key role in the altered biomechanics and resulting dysphonia associated with NPVH.

Pitch, loudness and quality of the voice are primarily controlled by laryngeal muscles in a complex process that is still not fully understood. The process involves the coordinated action of intrinsic and extrinsic muscles (Huber *et al.*, 2004), neural muscle effects (Titze *et al.*, 2002), and auditory and somatosensory feedback and feedforward mechanisms (Lester *et al.*, 2020). Though no mathematical model currently captures all of these factors, efforts have been made to describe components of laryngeal muscle control by either simplified biomechanical representations (Farley, 1996; Titze and Hunter, 2007; Titze and Story,

2002) or high-fidelity three-dimensional finite element models (Geng *et al.*, 2020; Gömmel *et al.*, 2007; Hunter *et al.*, 2004; Movahhedi *et al.*, 2021; Yin and Zhang, 2014). These high order models can capture the complex biomechanical and geometrical changes due to muscle activation but are likely too computationally demanding to account for neural motor control effects. Low-order models can better handle the latter task (Manriquez *et al.*, 2019) and are more suitable for comprehensive parametric simulations that would be needed in the context of laryngeal motor control. However, there is currently no muscle activation framework for low-order lumped-element models of the vocal folds that incorporates the possibility of independent co-contraction of all agonist/antagonist intrinsic muscle pairs.

The present study introduces a physiologically-based scheme for controlling the mechanical properties of a self-sustained, low-order model of the vocal folds through both independent and coordinated activation of all five intrinsic laryngeal muscles. The approach builds upon prior efforts that describe rules for controlling low-order models (Titze and Story, 2002), vocal fold posturing (Titze and Hunter, 2007), and a triangular body-cover vocal fold model (Galindo *et al.*, 2017). The scheme provides a flexible and physiologically relevant way to control the self-sustained, fully interactive voice production model for both sustained vowels and time-varying glottal gestures that enables the exploration of the role of antagonistic muscle pairs in phonation. In this study, we illustrate the capabilities of the proposed scheme and contrast the simulations against prior numerical and experimental studies. Future studies will be devoted to comprehensively exploring the range of vocal disturbances associated NPVH with the proposed scheme.

The paper is organized as follows. In [section II](#), the different components of the proposed model are introduced. In [section III](#), results are presented for posturing, steady and dynamic phonatory gestures, and antagonistic muscle behavior. In [section IV](#), the discussion of the results is provided, along with the proposed guidelines for future work. Finally, [section V](#) summarizes the work and provides the main conclusions of the study.

II. PHYSIOLOGICALLY-CONTROLLED VOICE PRODUCTION MODEL

Herein, we aim to simulate the muscle control exerted by the coactivation of the five intrinsic laryngeal muscles during phonation: cricothyroid (CT), thyroarytenoid (TA), lateral cricoarytenoid (LCA), interarytenoid (IA), and posterior cricoarytenoid (PCA); along with the passive contribution of the vocal ligament (LIG) and VF mucosa (MUC). Laryngeal function is described herein in terms of the glottal posture, resulting from the accommodation of the laryngeal cartilages, and of the VF oscillations around the phonatory configuration.

The main components of the proposed model are comprised of a VF posturing scheme, the triangular body-cover VF model, an extended set of physiological rules for the VF model, and a vocal tract model. Each component is introduced in this section and their interrelationships are described.

A. Vocal fold posturing model

Phonatory posturing refers to the large, slowly-varying changes (relative to VF oscillations) in the glottal geometry due to the accommodation of the surrounding structures and the mechanics of the laryngeal tissues, which can be described in terms of the relative

movement of the main laryngeal cartilages (see [Figure 1](#)). The cricoid cartilage is a ring-shaped structure that delimits the larynx inferiorly. It provides support anteriorly to the thyroid cartilage, a large shield-like structure forming the main anterior framework of the larynx, and posteriorly to the paired small pyramidal-shaped arytenoid cartilages. The anterior angle in each arytenoid, referred to as the vocal process (VP), serves as the posterior points of attachment for the VFs. Adduction/abduction comes from the movement of the arytenoid cartilages around the cricoarytenoid joint (CAJ), the anatomical link with the cricoid cartilage (see [Figure 1\(a\)](#)). Whereas adduction is controlled by the LCA, IA, and TA muscles, abduction is mainly controlled by the PCA muscle with minor contribution from the CT muscle ([Chhetri et al., 2012, 2014](#); [Geng et al., 2020](#); [Hunter et al., 2004](#)). On the other hand, the relative movement of the thyroid and cricoid cartilages around the cricothyroid joint (CTJ), as shown in [Figure 1\(b\)](#), is driven by the co-activation of the CT and TA muscles and plays a key role in VF elongation ([Chhetri et al., 2014](#); [Geng et al., 2020](#)).

The biomechanical model introduced by [Titze and Hunter \(2007\)](#) was applied to capture the main effects of the laryngeal musculature on the laryngeal configuration. A detailed description of the model development and the measurement of the biomechanical parameters can be found in Chapter 3 of [Titze \(2006\)](#). The model is built around the relative configuration of laryngeal cartilages; namely, that of the arytenoid cartilages with respect to the cricoid cartilage at the CAJ, and of the thyroid cartilage with respect to the cricoid cartilage at the CTJ. Phonatory configuration is described in a transverse plane at the glottal level (see [Figure 1\(a\)](#)). The global coordinate system is set with the y -axis along the midplane

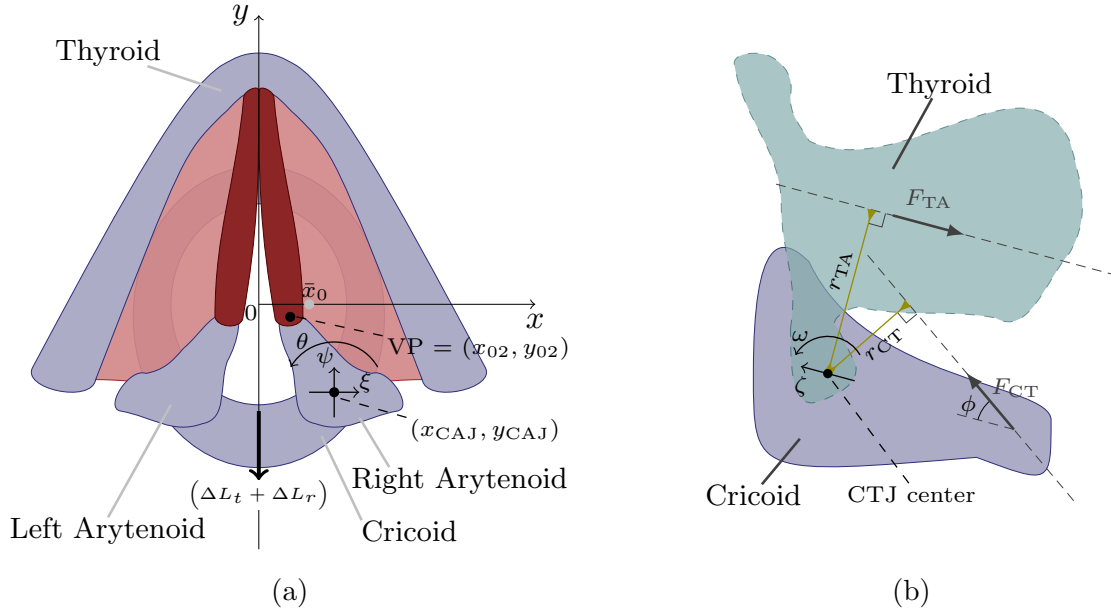


FIG. 1. (Color online) Main laryngeal structures involved in the prephonatory posturing. (a) Cricoarytenoid accommodation at the glottal plane; and (b) Projection of effective cricothyroid accommodation on the glottal plane. Glottal geometry and vocal fold adjustment are controlled via the relative accommodation of major laryngeal cartilages. Figures adapted from [Titze \(2006\)](#). CAJ: cricoarytenoid joint, CTJ: cricothyroid joint.

in the glottis, pointing anteriorly, and the x -axis passing through the vocal process in the 100
 cadaveric position, pointing to the right. Hence, the Cartesian coordinates of the right VP 101
 in the cadaveric state is $(\bar{x}_0, 0)$, and geometric symmetry across the midplane is henceforth 102
 assumed. 103

The complex movements involved in arytenoid accommodation are modeled as coordi- 104
 nated “effective” movements of translation and rotation relative to the fixed cadaveric CAJ 105
 center, (x_{CAJ}, y_{CAJ}) . Let (ξ, ψ) and θ be, respectively, the relative Cartesian displacements 106
 and the angle of rotation of the right arytenoid cartilage with respect to the CAJ center, 107

as described in [Figure 1\(a\)](#). The equations of motion are as follows ([Titze, 2006](#); [Titze and Hunter, 2007](#)):

$$M_{ac} \ddot{\xi} + d_x \dot{\xi} + k_x \xi = \sum_{i \in \mathcal{I}} \alpha_i F_i, \quad (1a)$$

$$M_{ac} \ddot{\psi} + d_y \dot{\psi} + k_y \psi = \sum_{i \in \mathcal{I}} \beta_i F_i, \quad (1b)$$

$$I_{ac} \ddot{\theta} + \delta \dot{\theta} + \kappa \theta = \sum_{i \in \mathcal{I}} \gamma_i F_i, \quad (1c)$$

where a dot over a variable indicates differentiation with respect to time, t . F_i denotes the point force magnitude for each element in the set of laryngeal tissues $\mathcal{I} = \{\text{LCA, IA, PCA, CT, TA, LIG, MUC}\}$, and α_i , β_i , and γ_i are the associated directional cosines and directional moment, as reported by [Titze and Hunter \(2007\)](#). Biomechanical parameters M_{ac} and I_{ac} are the mass and moment of inertia of the arytenoid cartilage; k_x , k_y , and κ are the translational and rotational stiffnesses (computed according to Chapter 3 in [Titze \(2006\)](#)); and d_x , d_y , and δ are the translational and rotational damping coefficients, respectively.

Following [Titze \(2006\)](#), the relative cricoid accommodation with respect to the thyroid cartilage is in turn simulated in terms of translational, ζ , and rotational, ω , movements around the fixed CTJ center, as illustrated in [Figure 1\(b\)](#). A simple scheme for projecting the effects of CT muscle activation on the horizontal glottal plane is considered, which allows assessment of the concomitant changes on the glottal configuration and vocal fold elongation. It is based on the following second-order equations:

$$M_{cc} \ddot{\zeta} + k_t (t_t \dot{\zeta} + \zeta) = [\cos \phi F_{CT} - (F_{TA} + F_{LIG} + F_{MUC})], \quad (2a)$$

$$I_{cc} \ddot{\omega} + k_r (t_r \dot{\omega} + \omega) = [r_{CT} F_{CT} - r_{TA} (F_{TA} + F_{LIG} + F_{MUC})], \quad (2b)$$

where M_{cc} and I_{cc} are the mass and moment of inertia associated with translation and 123
 rotation of the cricoid-arytenoid complex around the CTJ, k_t and k_r are the translational 124
 and rotational stiffnesses (computed according to Chapter 3 in [Titze \(2006\)](#)), t_t and t_r are 125
 the time constants for the translational and rotational viscous damping, r_{TA} and r_{CT} are the 126
 moment arms for the TA and CT torques relative to CTJ center, and ϕ is the angle between 127
 the line of action of F_{CT} and the translation axis of the cricoid cartilage, respectively. 128

Cricoid accommodation gives rise to a concomitant posterior displacement, $(\Delta L_t + \Delta L_r)$, 129
 in the arytenoid cartilage, as illustrated in [Figure 1\(a\)](#), where $\Delta L_t = \zeta$ and $\Delta L_r = r_{TA} \omega$ are 130
 the resulting posture effects due to the translation and rotation around the CTJ, respectively. 131
 As the VP is structurally linked to the arytenoid cartilage, its Cartesian coordinates are 132
 obtained as follows ([Titze and Hunter, 2007](#)): 133

$$x_{02} = x_{CAJ} - (x_{CAJ} - \bar{x}_0) \cos \theta + y_{CAJ} \sin \theta + \xi, \quad (3a)$$

$$y_{02} = y_{CAJ}(1 - \cos \theta) - (x_{CAJ} - \bar{x}_0) \sin \theta + \psi - (\Delta L_t + \Delta L_r). \quad (3b)$$

The contribution to vocal fold elongation due to arytenoid adduction is obtained by ([Titze 134
 and Hunter, 2007](#)): 135

$$\Delta L_a = -[y_{CAJ}(1 - \cos \theta) - (x_{CAJ} - \bar{x}_{02}) \sin \theta + \psi]. \quad (4)$$

Then, the total VF elongation is modeled as the sum of the translational, rotational, and 136
 adductory components, and thus the vocal fold strain is given by: 137

$$\epsilon = \frac{1}{L_0} (\Delta L_a + \Delta L_t + \Delta L_r), \quad (5)$$

where L_0 is the cadaveric VF length. Equation (5) dynamically couples the adduction and
 elongation procedures (Titze, 2006; Titze and Hunter, 2007). The elongated VF length is
 $L_g = (1 + \epsilon) L_0$.

In order to simulate the internal stress-strain response in the laryngeal tissues and to
 obtain the forces F_i , $i \in \mathcal{I}$, the modified one-dimensional Kelvin model of elongation is
 applied (Hunter and Titze, 2007; Hunter *et al.*, 2004). The modeled tissue force accounts
 for the active component due to the internal muscle contractile forces, and the passive
 response force in connective tissue. The activation level for each intrinsic muscle is then
 controlled through a normalized coefficient, i.e., $0.0 \leq a_i \leq 1.0$, for $i \in \{\text{LCA, IA, PCA,}$
 $\text{CT, TA}\}$. Because the vocal ligament and mucosa are non-contractile connective tissues,
 the active component is set to zero for $i \in \{\text{LIG, MUC}\}$. In Appendix A, the muscle model
 and the biomechanical parameters for the laryngeal tissues are described in more detail.

B. Triangular body-cover model of the vocal folds

The triangular body-cover model (TBCM) introduced by Galindo *et al.* (2017) is revised
 for numerically modeling the VF oscillations. Figure 2 provides a schematic of the TBCM
 model, with the associated tissue parameters and coordinates, where the subscripts u , l ,
 and b henceforth denote the upper, lower, and body masses, respectively. The VF model is
 based on the layered approximation proposed by Story and Titze (1995) for capturing the
 body-cover structure of the VFs, where two masses stacked in the inferior-superior direction
 model the cover and a single large mass situated laterally encapsulates the body dynamics.
 These lumped elements are coupled via non-linear mechanical elements to account for tissue

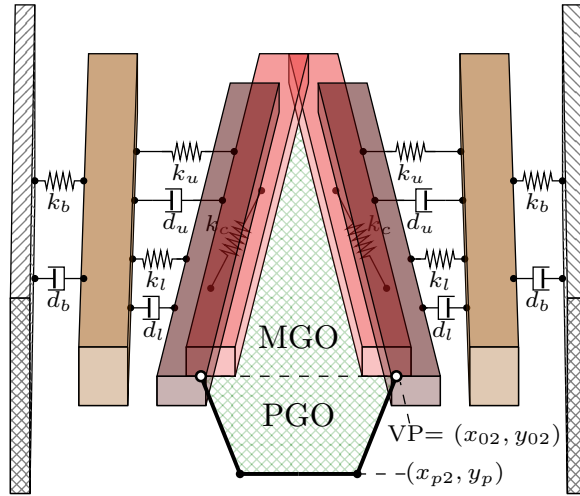


FIG. 2. (Color online) Schematic of the triangular body-cover model of the vocal folds.

viscoelasticity. In addition, the TBCM incorporates a gradual tilt of the VF edges in the 159
 anterior-posterior direction as a function of the degree of abduction, as is shown in Figure 2, 160
 giving rise to a triangular glottis accounting for the anatomical dorsal-ventral gradient in the 161
 VFs, and the zipper-like closure commonly observed in female phonation (Birkholz *et al.*, 162
 2011a,b). The TBCM formulation considers the structural link between the membranous 163
 area and the posterior glottal opening extended onto the cartilaginous glottis (Erath *et al.*, 164
 2013; Zañartu *et al.*, 2014). 165

Originally, the TBCM was built around the simplification that muscle control only af- 166
 fects the VF adjustment, so the arytenoid accommodation was independently parameterized 167
 through *ad hoc* rotation and displacement parameters. In this study, on the contrary, it is 168
 assumed that arytenoid accommodation is solved within the laryngeal posturing framework 169
 described in section II A. Hence, the adductory displacement in the posterior border of the 170
 upper mass, relative to the anterior commissure, coincides with the VP horizontal coordi- 171

nates x_{02} in Equation (3a) (see Figure 2). For the adductory displacement of the lower mass, x_{01} , the net glottal convergence is also considered following the ideas in Titze and Story (2002).

The coupled equations for simulating the TBCM dynamics are:

$$F_u = m_u \ddot{x}_u = F_{k,u} + F_{d,u} - F_{kc} + F_{e,u} + F_{Col,u}, \quad (6a)$$

$$F_l = m_l \ddot{x}_l = F_{k,l} + F_{d,l} + F_{kc} + F_{e,l} + F_{Col,l}, \quad (6b)$$

$$F_b = m_b \ddot{x}_b = F_{k,b} + F_{d,b} - [F_{k,u} + F_{d,u} + F_{k,l} + F_{d,l}], \quad (6c)$$

where m is mass, x is the medial-lateral displacement over time, and F is the force component for each block. Rest positions for the upper and lower blocks are $x_{u,0} = 0.5 x_{02}$, $x_{l,0} = 0.5 x_{01}$ pursuant to VF posturing, whereas $x_{b,0} = 3$ mm (Galindo *et al.*, 2017). Furthermore, force subscripts k , d , e , and kc represent the mechanical forces produced by the springs, dampers, flow pressures, and elastic coupling between the upper and lower masses, respectively. An additional spring force, F_{Col} , is introduced during vocal fold collision to capture the effects of impact between opposing upper/lower cover masses. The definitions of the forces are described in detail in the appendix of Galindo *et al.* (2017), and are thus omitted here for brevity. To compute the aerodynamic driving forces, the intraglottal pressures on the upper/lower cover masses are derived from the subglottal pressure, P_s , and the supraglottal pressure, P_e , according to the formulation introduced in the appendix of Titze (2002).

C. Physiological rules for the triangular body-cover model

187

The empirical rules introduced by [Titze and Story \(2002\)](#) are applied and extended for 188
the computation of the TBCM parameters. These rules introduce dynamic muscle control 189
based on mapping the normalized activation levels of the intrinsic muscles, introduced at 190
the end of [section II A](#), into the relevant mechanical parameters (e.g., linear stiffness, mass 191
distribution, glottal convergence, and VF length, thickness, and depth). Besides controlling 192
the TBCM vibrations, the rules also have an impact on other aerodynamic and acoustic 193
quantities in scenarios involving the tissue-flow-acoustic interaction in the glottis ([Lowell 194
and Story, 2006](#); [Zañartu et al., 2014](#)). 195

Originally, [Titze and Story \(2002\)](#) begin by prescribing the VF elongation and VP ad- 196
duction as a function of normalized activation levels a_{TA} , a_{CT} , and a_{LC} , with the latter 197
combining the effects of both the LCA and PCA muscles. The geometrical parameters and 198
fiber stresses are then obtained from the VF elongation, after which the stiffness and mass 199
distributions in the VF model are computed. In this work, a few methodological modi- 200
fications are considered to extend the rules for the TBCM. The first difference consists of 201
including independent activation levels for the five intrinsic muscles; hence, the activation set 202
 $\mathbf{a} = [a_{LCA}, a_{IA}, a_{PCA}, a_{CT}, a_{TA}]$ controls the activation of the laryngeal musculature. More- 203
over, internal stresses in the VF tissues, specifically for the TA muscle, *LIG*, and *MUC*, are 204
dynamically obtained by solving a modified Kelvin model (see [Appendix A](#)), whereas the 205
VF elongation and VP adduction are obtained from the laryngeal posturing according to 206
Equations (5) and (3a), respectively; hence, the elongation and adduction rules in ([Titze 207](#)

and Story, 2002) are replaced. With this information, the remaining rules in Titze and Story (2002) are thus applied for computing the nodal point, thickness, and depth for each block and glottal convergence, from which the biomechanical parameters (i.e., mass and spring values) of the TBCM are derived. Notably, the shear moduli of the body and cover are set to $\mu_b = 600$ Pa and $\mu_c = 300$, respectively, which differs from the values selected by Titze and Story (2002).

Based on VF adduction and symmetry with respect to the midsagittal plane, the glottal area for the upper and lower cover masses are:

$$A_u = 2(1 - \alpha_u)L_g(\tilde{x}_u + 0.5(1 + \alpha_u)x_{01}), \quad (7a)$$

$$A_l = 2(1 - \alpha_l)L_g(\tilde{x}_l + 0.5(1 + \alpha_l)x_{02}), \quad (7b)$$

where $\tilde{x}_u = x_u - x_{u,0}$ and $\tilde{x}_l = x_l - x_{l,0}$ are block displacements relative to their rest positions. Additionally, α_u and α_l are the proportions of mass length for the upper and lower blocks undergoing collision at the given time, where $0.0 \leq \alpha_u, \alpha_l \leq 1.0$. As a result, the area for the membranous glottal opening is $A_{MGO} = \min\{A_u, A_l\}$. The effects of laryngeal posture on the posterior cartilaginous portion of the glottis are also simulated. Following Titze (2006), a trapezoidal shape is assumed for the posterior glottal opening, thus the resulting area can be computed as follows:

$$A_{PGO} = \max\{0, \min\{(x_{p1} + x_{01}), (x_{p2} + x_{02})\}(y_{02} - y_p)\}, \quad (8)$$

where x_{p1} is the posterior wall half-width at the bottom, x_{p2} is the posterior wall half-width at the top, and y_p is the posterior wall position along the longitudinal axis. The total glottal

area comprises both the membranous and the cartilaginous parts:

$$A_g = A_{\text{MGO}} + A_{\text{PGO}}. \quad (9)$$

D. Interactions at the glottis and acoustic wave propagation

To capture the physics of human phonation, the three-way interaction between sound, flow, and VF tissue is considered. For computing the air volume velocity, U_g , through the glottal area, A_g (see Equation (9)), the solver proposed in [Zañartu *et al.* \(2014\)](#) considering the acoustic driving pressures and the posterior glottal opening is applied, with the inclusion of the corrections made by [Lucero and Schoentgen \(2015\)](#). As shown in [Zañartu *et al.* \(2014\)](#), in the one-dimensional flow approximation the solution obtained for a domain with two separate orifices for the posterior and membranous areas is equivalent to solving for the volume velocity through the total glottal area, A_g .

The wave reflection analog scheme is selected for describing the propagation of one-dimensional, planar acoustic waves in the time domain throughout the equivalent subglottal and supraglottal systems ([Zañartu, 2006](#)). These tracts are discretized as the concatenation of a finite number of short uniform cylinders with variable cross-sectional areas. The area functions obtained from magnetic resonance imaging data for a male participant during sustained phonation are applied to simulate the supraglottal tract for different vowels ([Story, 2008](#)) and the subglottal system ([Zañartu, 2006](#)). For simulating an equivalent excised-larynx scenario within the same framework, the non-interactive control scenario introduced by [Titze and Palaparthi \(2016\)](#) is also considered, where a very wide cross-sectional area (30 cm²) is set for every cylinder in both the subglottal and the supraglottal systems. Boundary

conditions based on a resistive lung termination and a parallel resistive-inertive element at 245
the lips are also defined in the simulations. 246

E. Numerical implementation 247

The implemented model involving the muscle control of the larynx posture and vocal fold 248
function depends upon several anatomical and biomechanical parameters. Model parameters 249
were selected to simulate the physiology of male phonation. The parameters considered in 250
this work are reported in Table I. As in Galindo *et al.* (2017), the simulations were performed 251
using a truncated Taylor-series approximation to solve the differential equations. A sampling 252
frequency of 44.1 kHz was employed. A colored random source component was included for 253
modeling the turbulent aspiration noise generated at the glottis (Galindo *et al.*, 2017). 254

III. RESULTS 255

This section introduces illustrative simulations with the proposed voice production model. 256
The effects of intrinsic muscle activation on the laryngeal posture are first described, then 257
simulations for sustained vowels and articulatory gestures are subsequently analyzed. An 258
example resembling antagonistic muscle behavior during sustained phonation is also dis- 259
cussed. 260

A. Vocal fold posturing

261

The biomechanical scheme for the prephonatory laryngeal posturing utilizes, principally, 262
the arytenoid cartilage accommodation for controlling glottal adduction and abduction. 263
Figure 3 shows the effect of the individual activation of the five intrinsic muscles on the 264
(right) arytenoid posture, as described by the position of the cricoarytenoid joint and the 265
vocal process. Figure 3 also includes an equivalent LCA/IA *adductory* complex given by 266
 $a_{LCA} = a_{IA} = a_{Add}$, i.e., the coupled 1:1 activation for LCA and IA muscles, as in previous 267
studies (Chhetri *et al.*, 2012, 2014; Geng *et al.*, 2020; Palaparthi *et al.*, 2019). The muscle 268
activation is incremented in normalized steps of 0.1 from 0 to 1 for each case. Note that the 269
displacement of the cricoarytenoid joint is smaller and different in nature than those of the 270
vocal process. 271

Herein, VF adduction is characterized by the medialization and (positive) counter- 272
clockwise rotation of the arytenoid cartilage, and is controlled by the LCA muscle and, 273
to a lesser extent, the TA muscle. Glottal abduction is achieved via the PCA muscle 274
where concurrent vocal process lateralization and clockwise arytenoid rotation is observed. 275
Furthermore, anterior-posterior displacements of the vocal process are determined by the 276
antagonist effects of the TA and CT muscles. Although activation of the IA muscle min- 277
imally alters the position of the vocal process, it does displace the cricoarytenoid joint 278
medially and caudally, thus reducing the posterior glottal opening. The adductory complex 279
combines both the LCA and IA muscles, thus allowing for jointly reducing the membranous 280
and posterior glottal areas. 281

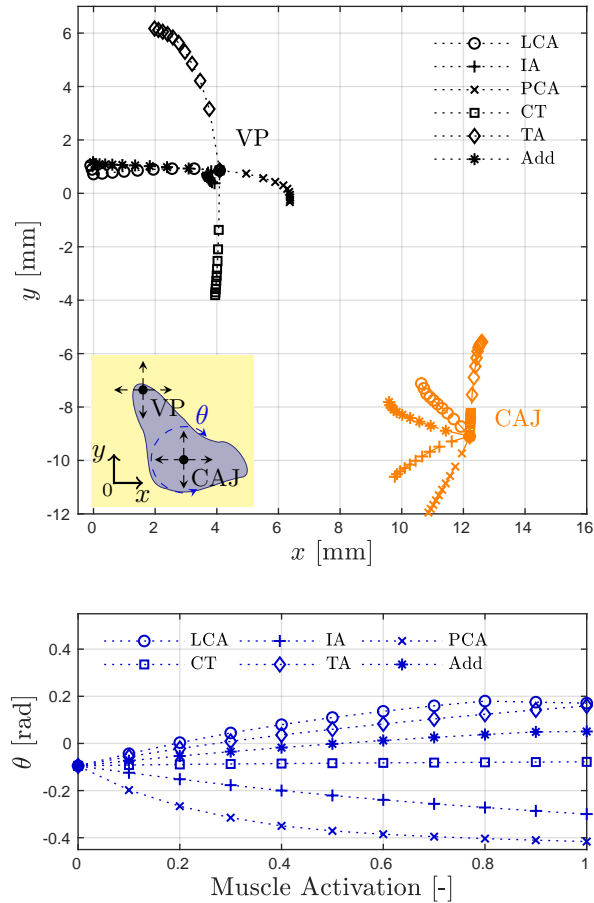


FIG. 3. (Color online) Simulated accommodation of the (right) arytenoid cartilage obtained by the independent activation of the five intrinsic muscles and the adductory complex. *Top*: Cartesian displacement of the cricoarytenoid joint (CAJ) center, $(x_{CAJ} + \xi, y_{CAJ} + \psi)$, and the vocal process (VP), (x_{02}, y_{02}) . The inset schematic illustrates the VP movements resulting from the displacement and rotation of the CAJ. *Bottom*: Rotation angle θ for the CAJ. Concurrent beginning of the paths indicates zero muscle activation.

The effects on VF adduction due to muscle coactivation in the model are illustrated in 282
 Figure 4. The resulting movement of the vocal process (refer to the attached schematic) 283
 from the incremental activation of the adductory complex is shown for different coactivation 284

states of the remaining muscles. For each path, activation levels for a_{Add} increased from 285
 0 to 1 in normalized steps of 0.1. The resulting movement of the vocal process with no 286
 coactivation is drawn in black in the center of the figure, whereas the two topmost black 287
 paths and the two bottommost black paths describe the coactivation with the TA and CT 288
 muscles, respectively. Results involving two cases of PCA coactivation are also included for 289
 contrast. 290

These results further illustrate the antagonist role of the TA and CT muscles, where 291
 ventral and dorsal displacements of the vocal process are produced via the activation of the 292
 TA and CT muscles, respectively, and where the TA muscle increases the total adduction 293
 of the vocal process. Moreover, [Figure 4](#) also illustrates that coactivation of the PCA 294
 muscle introduces a noticeable lateral displacement in the vocal process path with increasing 295
 activation, and slightly changes the direction of its path. 296

In [Figure 5](#), muscle activation maps depicting VF elongation and vocal process distance 297
 for pairs of intrinsic muscle groups are presented. VF elongation is computed by Equation 298
 (5), whereas the distance between the vocal processes is measured with respect to the rest 299
 distance at zero muscle activation. A coupled 1:1 activation was applied for every muscle 300
 in a group, for example, an activation level \bar{a} set to group LCA/IA implies $a_{LCA} = a_{IA} =$ 301
 \bar{a} . The coactivation of the main phonatory laryngeal muscles is investigated in [Figure 5](#), 302
 whereas the effect of PCA activation is described further bellow. Similar representations have 303
 been applied in the past for investigating muscle groups having antagonistic or synergistic 304
 functions in VF posturing in experiments with excised canine larynges, ([Chhetri et al., 2012,](#) 305
[2014](#)), and in simulations involving a three-dimensional finite element model of a canine 306

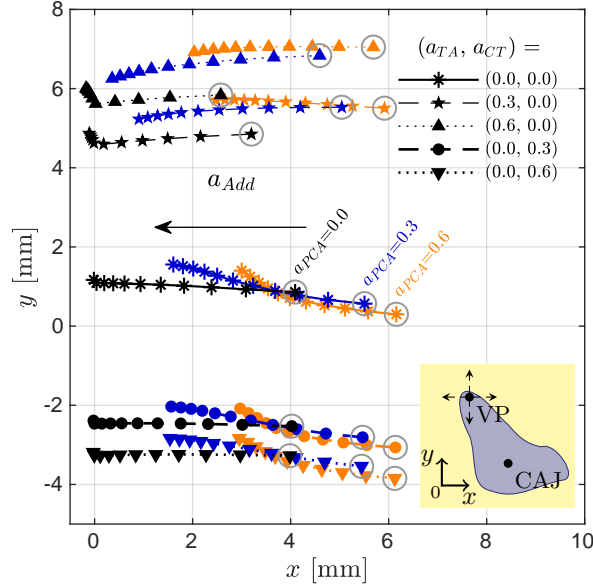


FIG. 4. (Color online) Effects of laryngeal muscle coactivation on glottal adduction. Vocal process (VP) coordinates, (x_{02}, y_{02}) , produced through the activation of the adductory complex for the non-coactivation case (solid line with medium markers), and for two activation levels for both TA muscle (dashed and dotted lines with small markers) and CT muscle (dashed and dotted lines with large markers). Three PCA activations are drawn in black ($a_{PCA} = 0.0$), dark color ($a_{PCA} = 0.3$), and light color ($a_{PCA} = 0.6$) lines. Markers enclosed in circles indicate the results for null adductory complex activation ($a_{Add} = 0.0$). The inset schematic illustrates the VP Cartesian movements.

larynx (Geng *et al.*, 2020). Given that the proposed biomechanical model of the larynx 307
 was partially based on canine models (Titze and Hunter, 2007), contrast against these prior 308
 studies is feasible and meaningful. 309

Results for VF elongation (from VF strain in the left column of Figure 5) show that 310
 the proposed model captures the antagonistic effects of the CT and TA muscles, where 311
 VF strain can be increased/decreased through corresponding CT/TA muscle activations. It 312

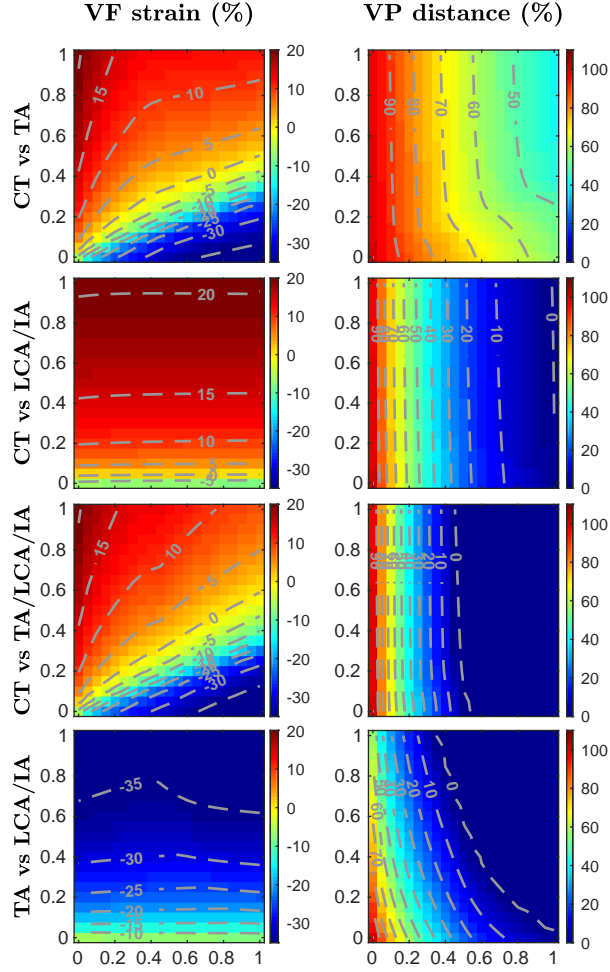


FIG. 5. (Color online) Muscle activation plots for parametric coactivation of main phonatory intrinsic muscles. Vocal fold strain (left column) and vocal process distance (right column) are depicted as functions of the paired coactivation of muscle groups. The rows show four activation scenarios with contour lines included for clarity. For each row, A vs B refers to the abscissa and ordinate axes indicating activation levels for muscle groups A and B, respectively; null activations are set for the remaining intrinsic muscles.

can be observed that the main adductor muscles have a minor effect on VF elongation. The 313
largest VF elongation (around +20%) is obtained from maximum CT activation and zero TA 314
activation. Similar strain values were obtained in simulations using finite element models 315
(Geng *et al.*, 2020), whereas studies with canine models have reported larger elongation 316
values (Chhetri *et al.*, 2012, 2014). In contrast, the shortest VF elongation results from 317
maximum TA activation and zero CT activation. The minimum VF strain values (around 318
-35%) are lower than those reported in the benchmark studies. However, the strain contour 319
lines for all activation conditions resemble the diagonal patterns reported by other authors 320
(Chhetri *et al.*, 2012; Geng *et al.*, 2020). 321

Vocal process distance indicates the adduction of the vocal folds. The plots in Figure 5 322
show the resulting values for the distance between the vocal processes, measured in per- 323
centage relative to the distance at rest (i.e., null activation for all intrinsic muscles). As 324
expected, a strong synergistic adductory role played by the TA, LCA, and IA muscles is 325
noticeable. Individual TA activation has a less significant effect on glottal adduction than 326
the coactivation of the LCA/IA complex. However, the equal activation of the TA, LCA, 327
and IA muscles as a group compresses the previous gradual posturing of the vocal processes 328
at the region of lower activation levels. Despite the considerable anatomical and functional 329
oversimplifications in the biomechanical model of the larynx, our simulations of vocal pro- 330
cess distance are in agreement with previous experimental and high-order modeling studies 331
(Chhetri *et al.*, 2012, 2014; Geng *et al.*, 2020). Two important differences are worth noting. 332
First, the previous studies indicate that a non-zero vocal process distance is obtained even 333
for strong cases of glottal adduction (Geng *et al.*, 2020; Moisik and Gick, 2017). The im- 334

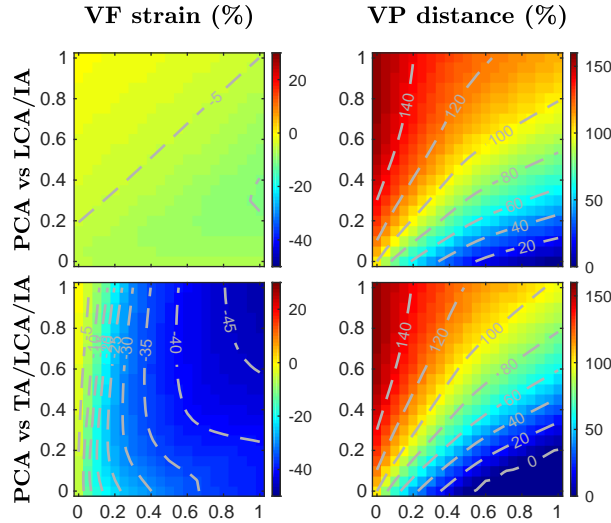


FIG. 6. (Color online) Muscle activation plots for parametric coactivation of adductory/abductory intrinsic muscles. Vocal fold strain (left column) and vocal process distance (right column) are depicted as functions of the paired coactivation of muscle groups. The rows show two activation scenarios with contour lines included for clarity. For each row, A vs B refers to the abscissa and ordinate axes indicating activation levels for muscle groups A and B, respectively; null activations are set for the remaining intrinsic muscles.

plemented model, however, produces zero distance values for a range of muscle activation 335
 conditions. In addition, the current laryngeal model is not capable of reproducing the ab- 336
 ductory effect of the CT muscle on VF adduction reported by other authors (Chhetri *et al.*, 337
 2012, 2014; Geng *et al.*, 2020). 338

The PCA muscle is the main larynx abductor, with a key role during inspiratory laryngeal 339
 movements, whereas during typical phonation, it plays only a minor role (Poletto *et al.*, 340
 2004). Muscle activation plots portraying the VF elongation and vocal process distance 341
 for adductory/abductory antagonist muscle groups are depicted in Figure 6, following the 342

above methodology. The first row shows the results from the coactivation of the PCA 343
muscle versus LCA/IA group. It is observed that the distance between the vocal processes 344
ranges from nearly 0% for full activation of the LCA/IA group and no activation of the 345
PCA muscle, to around 150% for the opposite case, whereas the changes in VF strain are 346
minimal. Notice that, in the case of equal activation, the abductor force from the PCA 347
muscle is slightly superior to the antagonist force produced by combining the LCA and IA 348
muscles. The second row illustrates the results obtained by including the TA muscle in the 349
adductor group. The results show that the TA muscle acts to reinforce the adductor forces 350
that are opposite to the PCA muscle action, producing an appreciable region with null vocal 351
process distance; moreover, TA muscle inclusion yields a dramatic VF shortening of up to 352
-45 % strain for full activation of the four muscles considered. Further comparisons depict 353
that the PCA and CT muscles actuate differently during larynx accommodation, providing 354
evidence of no antagonist effect; the PCA muscle abducts the vocal process producing no 355
appreciable change in VF strain, whereas the CT muscle mainly elongates the VF with 356
a minimal modification of the distance between the vocal processes. This results are not 357
included here for conciseness. 358

B. Sustained phonatory gestures 359

Sustained vowel simulations are performed to investigate basic glottal function (self- 360
sustained oscillation and pitch) as a function of the laryngeal muscle activation and sub- 361
glottal pressure, P_s . For simplicity, the prephonatory laryngeal posture is fixed through the 362
constant activations $a_{LCA} = a_{IA} = 0.5$ and $a_{PCA} = 0.0$ for the main adductor/abductor 363

muscles, whereas VF adjustment is controlled via the parametric activation of a_{CT} and a_{TA} 364
 in the range from 0 to 1. 365

For each condition, 600 ms of simulated phonation data were obtained. In general, 366
 the simulations evidenced transients and fluctuations at the beginning, which were not 367
 relevant for the present analysis; thus, the first portion of data was discarded and only the 368
 last 200 ms steady segment was considered. An autocorrelation method was applied for 369
 assessing periodicity and fundamental frequency for the simulated glottal area waveform, 370
 A_g (Mehta *et al.*, 2015). In Figure 7, muscle activation plots are shown for fundamental 371
 frequency as a function of TA and CT muscle coactivation, for three physiological subglottal 372
 pressure levels $P_s = [0.8, 1.4, 2.0]$ kPa. Acoustic coupling for vowels $\{/æ/, /i/, /a/, /u/,$ 373
 $/o/, /e/\}$ as well as for a non-interactive acoustic system was also considered to further 374
 assess the model behavior. Results show that in the low subglottal pressure condition 375
 increasing CT activation leads to less stable, or even unachievable, VF oscillations (shown 376
 as blank portions in Figure 7). Self-sustained oscillations are strengthened by increasing 377
 the subglottal pressure level. The relation between high CT activation and phonation onset 378
 pressure has been described in excised larynx experiments (Chhetri *et al.*, 2014), as well 379
 as in high-order simulations (Palaparthi *et al.*, 2019). Results also show that the acoustic 380
 coupling facilitates self-sustained VF oscillations and raises pitch in comparison with the no 381
 vocal tract (non-interactive) scenario, where an increased region without periodic vibrations 382
 was observed. 383

Fundamental frequency contours resulting from coactivation of the TA and CT muscles 384
 globally resemble those reported in Titze and Story (2002) and Lowell and Story (2006). 385

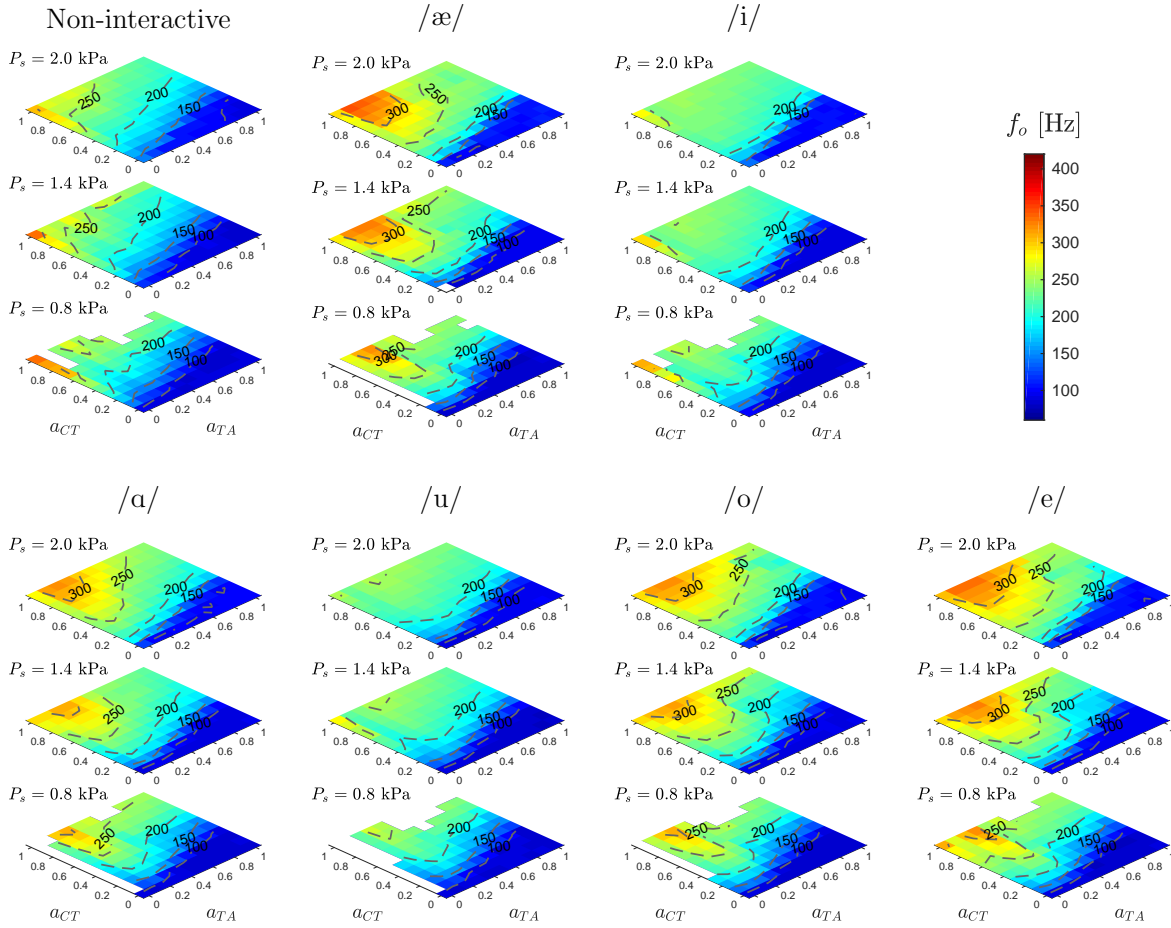


FIG. 7. (Color online) Muscle activation plots with fundamental frequency for CT versus TA activation, considering different vocal tract shapes and subglottal pressures $P_s = [0.8, 1.4, 2.0]$ kPa. In all the cases $a_{LCA} = a_{IA} = 0.5$, and $a_{PCA} = 0.0$. The non-interactive case has no vocal tract and represents an excised larynx scenario. Isofrequency contours are drawn for clarity.

CT activation is the main contributor to changes in fundamental frequency and the highest 386
 values are obtained for low values of TA activation. This result was expected and it has 387
 been reported before (Lowell and Story, 2006; Titze and Story, 2002). However, the original 388
 rules for muscle control of the body-cover VF model yield fundamental frequencies greater 389
 than 500 Hz, whereas the frequency range in Figure 7 is more restricted, showing maximum 390

values around 350 Hz. Fundamental frequencies up to 400 Hz are obtained for scenarios with 391
increased gottal adduction. In addition, prior reported muscle activation plots featured a 392
noticeable downward bending of the contour lines in the lower left region (low CT and TA). 393
The implemented model also shows this non-linear response for the fundamental frequency 394
in the region of weak TA activation and moderate-to-strong CT activation; however, bending 395
in the contour lines are less pronounced in comparison with the results reported by [Titze](#) 396
[and Story \(2002\)](#). This is more noticeable for the non-interactive vocal tract case. 397

C. Dynamic phonatory gestures 398

Simulations of dynamic (articulatory) gestures combine posturing and phonation and are 399
key to assessing the overall performance of the model. Simulations of repetitive voicing- 400
devoicing gestures, i.e., /hi-hi-hi-hi/, are shown in [Figure 8](#). Model parameters are set to 401
produce a modal male voice, where $P_s = 800$ Pa, $a_{TA} = 0.2$, $a_{CT} = 0.1$, and $a_{PCA} = 0.0$, for 402
a (male) vowel /i/ for a direct comparison with [Titze and Hunter \(2007\)](#). 403

As before, the equivalent LCA/IA adductory complex is controlled in time with $a_{LCA} =$ 404
 $a_{IA} = a_{Add}$. The three columns in [Figure 8](#) show simulations for weak (left), moderate (mid- 405
dle), and strong (right) VF adduction, respectively. Top panels depict the muscle control 406
signal a_{Add} for every case, with peak amplitude indicating the adduction level. Waveform 407
outputs of glottal area A_g , glottal volume velocity U_g , and radiated pressure P_o for the three 408
simulated adduction strengths are shown in the following three rows, respectively. Spectro- 409
grams describing time-frequency content for the radiated pressure signals are included in 410
the bottom row. 411

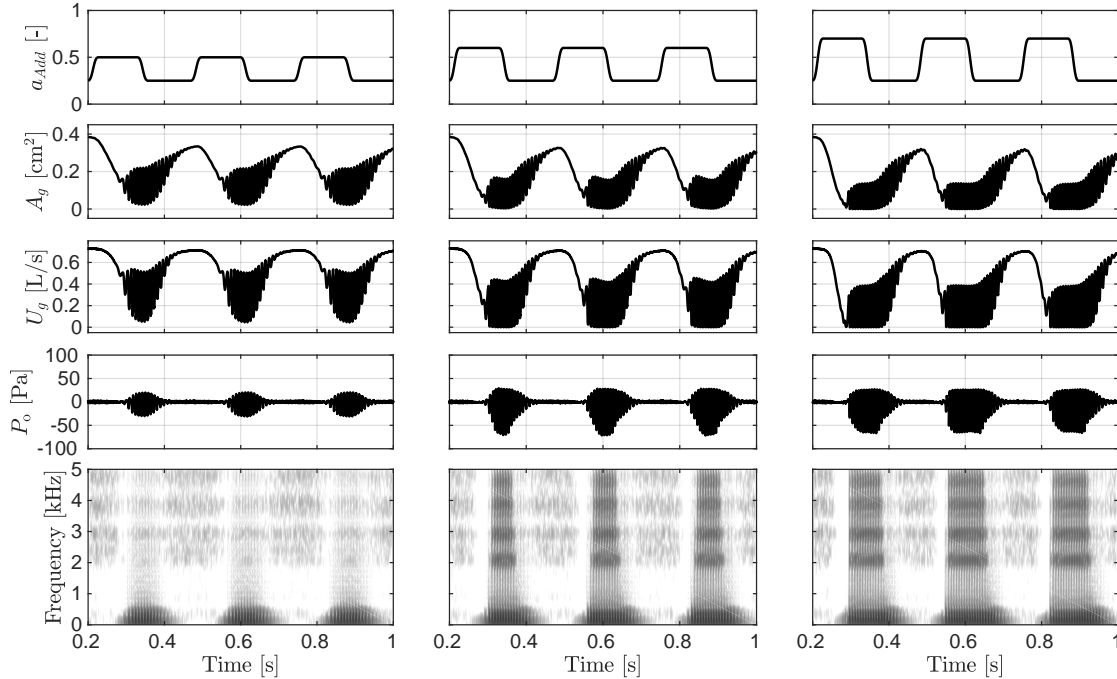


FIG. 8. Simulated muscle control of voicing-devoicing for a /hi-hi-hi-hi/ gesture. From left to right, columns correspond to simulations for weak, moderate, and strong VF adduction with maximum activation levels 0.5, 0.6, and 0.7, respectively. Adductory signals a_{Add} are shown in the top row. The following three rows show the output signals for the glottal area A_g , glottal volume velocity U_g , and the radiated acoustic pressure P_o . The bottom row depicts the wideband spectrogram of P_o .

Despite the overly simple and fairly square activation signals, the simulated variables 412
 capture the gradual VF adduction/abduction characteristic of the voicing/devoicing gesture. 413
 The noticeable delay in area and airflow waveforms with respect to variations in the control 414
 signal, a_{Add} , is a product of the combined effects of inertia in the biomechanical model of 415
 the larynx and the time constants in the laryngeal tissue model. Radiated sound pressure is 416
 further delayed as a consequence of acoustic wave propagation throughout the vocal tract. 417

Changes in VF adduction are primarily seen in the voice onset time and, to a lesser extent, 418
in the voice offset time. A higher magnitude in a_{Add} speeds up the onset of VF oscillations 419
and delays the offset of voicing. VF adduction condition also affects phonation time and the 420
spectral richness of the radiated sound. The latter is in accordance with previous studies 421
illustrating that, for a constant driving pressure, weak to moderate adduction conditions 422
modify PGO area in the range of small to large, which in turn produces a considerable 423
reduction of the radiated sound pressure level (Galindo *et al.*, 2017; Zañartu *et al.*, 2014). 424

Note that simulations are built around muscle control signals for the LCA and IA muscles 425
only. However, it is well known that during speech production all the laryngeal muscles 426
coactivate in complex ways (Moisik and Gick, 2017; Movahhedi *et al.*, 2021; Zhang, 2016). 427
As illustrated before, other muscles, such as PCA, TA, and CT, have an effect on VF 428
adduction and can also alter voicing onset and offset (Poletto *et al.*, 2004; Titze and Hunter, 429
2007). The proposed model allows for incorporating all five muscle activations in a time 430
varying fashion, which can improve the physiological relevance when modeling articulatory 431
gestures. Nevertheless, the resulting output with the simplified muscle control input is still 432
in agreement with Titze and Hunter (2007) and Poletto *et al.* (2004). 433

D. Antagonistic muscle behavior 434

As the proposed model allows for analyzing the effects of selected levels of antagonistic 435
muscle activation, we herein simulate conditions that have the same vocal fold posturing, but 436
with different underlying antagonistic muscle activations. We argue that this exercise can 437

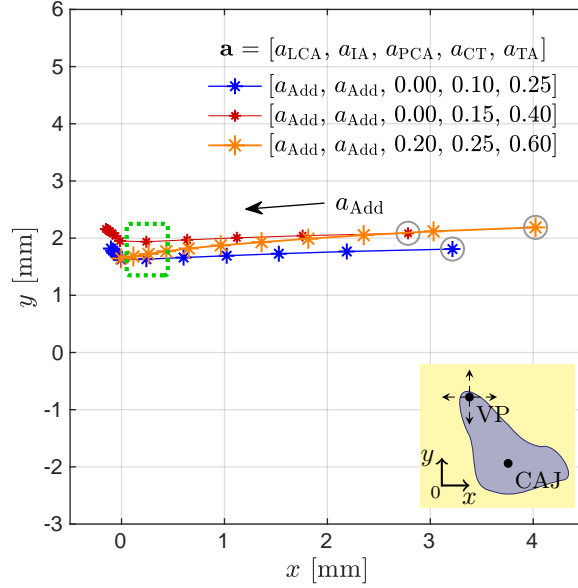


FIG. 9. Displacement paths for the right vocal process (VP), (x_{02}, y_{02}) , for three simulated tension states in the larynx. Trajectories correspond to laryngeal postures produced by parametric activation of the intrinsic muscles following the activation set $\mathbf{a} = [a_{LCA}, a_{IA}, a_{PCA}, a_{CT}, a_{TA}]$. The paths describe variations for the normalized activations a_{Add} in the range of 0 to 1 in steps of 0.1. The inset schematic illustrates the VP Cartesian movements. Configurations enclosed in the dotted rectangle are considered for voiced sound simulations.

lead to future studies exploring disproportionate coactivation of antagonist intrinsic muscles 438
 that can be related to NPVH. 439

The ability of the model to attain the same prephonatory VF posturing for various muscle 440
 activation conditions is illustrated in Figure 9, where the displacement paths for the right 441
 vocal process for three simulated laryngeal conditions are drawn. The dotted rectangle in 442
 Figure 9 shows that three distinctly different activation conditions (reported in Table II) 443
 can produce almost the same vocal process position, and result in a visually similar VF 444

configuration. This idea can also be extended into paths of glottal adduction. [Figure 9](#) 445
 shows three paths obtained when varying the adductory complex a_{Add} that correspond to 446
 different activations of all intrinsic muscles. These paths compare a given prephonatory 447
 state with two other conditions involving lower and higher activation levels, respectively. 448
 A slight increase in abduction is seen in the latter case for each marker (displacement to 449
 the right) do to PCA activation; although the paths overlap, this indicator shows that the 450
 increased tension scenario yields a more abducted condition for every step. 451

Even though VF posturing can be visually preserved, changes in muscle activation are ex- 452
 pected to alter the TBCM parameters differently and, thus, the resulting vocal function. To 453
 investigate this idea, sustained phonation is simulated for the three activation sets (denoted 454
 as \mathbf{a}_I , \mathbf{a}_{II} , and \mathbf{a}_{III} in [Table II](#)) that result in the same VF posture although associated with 455
 different degrees of coactivation of the antagonist intrinsic muscles. For these simulations, 456
 a driving pressure $P_s = 800$ Pa is applied, and tract area functions for ten different vowels. 457

To describe multiple aspects of vocal function for each set, various parameters were 458
 computed, including 1) VF posturing: VF strain, vocal process distance, and membranous 459
 and posterior portions of the glottal area; 2) VF kinematics: fundamental frequency, open 460
 quotient (OQ), and closing quotient (CIQ); 3) Glottal aerodynamics: unsteady glottal airflow 461
 (AC Flow), stable glottal flow (DC Flow), maximum flow declination rate (MFDR), and 462
 amplitude of the first harmonic relative to the second harmonic ($H_1 - H_2$); 4) Voice acoustics: 463
 sound pressure level (SPL), and low-to-high (L/H) spectral ratio. These measures have been 464
 shown to be valuable for the assessment of vocal hyperfunction ([Cortés et al., 2018](#); [Galindo 465](#)
[et al., 2017](#); [Mehta et al., 2019, 2015](#); [Zañartu et al., 2014](#)). 466

The resulting measures of vocal function are reported in [Table III](#). As expected, given 467
that the vocal process position is almost the same, the parameters describing the laryngeal 468
posture are similar for the three conditions; the only evident difference is the increased PGO 469
area for set \mathbf{a}_{II} that results from the lower activation of the LCA and IA muscles. Moreover, a 470
significant increase in the minimum glottal area is observed for the \mathbf{a}_{II} condition, which leads 471
to a higher DC Flow. Kinematic measures in [Table III](#) show that fundamental frequency 472
and closing quotient show minor changes with the activation conditions, whereas OQ is 473
noticeably increased for the \mathbf{a}_{II} condition. 474

Aerodynamic measures in [Table III](#) show that the highest MFDR values are obtained, as 475
expected, for the more adducted cases, i.e., with less PGO leakage. Conversely, increasing the 476
PGO area decreases MFDR, suggesting less efficient acoustic excitation. Interestingly, AC 477
Flow and $H_1 - H_2$ show minor variations, suggesting negligible differences in the vocal tract 478
coupling and the source spectral tilt. In addition, acoustic measures provide complementary 479
evidence of the reduced phonatory efficiency for set \mathbf{a}_{II} , yielding a noticeable decrease of SPL 480
levels together with increased L/H spectral ratios, which are signs of less spectral energy in 481
the high frequency region. 482

IV. DISCUSSION 483

The proposed scheme allows for controlling prephonatory posturing and phonatory ges- 484
tures in a triangular body-cover model of vocal folds by means of the independent activation 485
of all of the intrinsic laryngeal muscles. It combines prior efforts to model laryngeal pos- 486
turing ([Titze and Hunter, 2007](#)), empirical rules relating muscle activation to biomechanical 487

parameters in a lumped-element model (Titze and Story, 2002), and a triangular body-cover 488
VF model (Galindo *et al.*, 2017). The scheme thus provides a flexible and physiologically 489
relevant way to control the self-sustained fully interactive voice production model for both 490
sustained vowels and time-varying glottal gestures. As a result, the approach allows for 491
exploring the role of antagonistic muscle pairs in phonation, which has direct implications 492
for studying normal and disordered muscle behavior in phonation. 493

In this study, it was first shown that the implemented framework can reproduce prior 494
findings with excised larynx experiments and high-order numerical simulations for sustained 495
vowels and simple articulatory gestures. In addition, we applied the approach to exemplify 496
the role of antagonistic muscle pairs and the effects of antagonistic muscle activation in 497
the context of a common manifestation of NPVH, with simulations in agreement with prior 498
clinical data. Thus, despite its low-order complexity, the scheme provides a physiologically- 499
inspired tool that could be used to gain insights into the physical mechanisms underlying 500
intrinsic muscle function in phonation. This becomes particularly useful for extending pre- 501
vious efforts to model vocal hyperfunction (Galindo *et al.*, 2017; Zañartu *et al.*, 2014) to 502
account for elevated, unbalanced, and poorly regulated activity of the intrinsic laryngeal 503
muscles, as seen in NPVH (Hillman *et al.*, 2020). We hypothesize that NPVH is associated 504
with a disproportionate coactivation of antagonist intrinsic muscles that result in a more 505
abducted prephonatory VF posturing, that in turn results in a reduced loudness that is com- 506
pensated with elevated subglottal pressure and further muscle tension. Subsequent efforts 507
will explore the use of the proposed model to investigate these ideas and aid in delineat- 508
ing the etiology and pathophysiology of vocal hyperfunction. The model has also potential 509

for developing improved estimation frameworks based on biomechanical models of human 510
phonation applicable to the prevention and treatment of VH (Alzamendi *et al.*, 2020; Ibarra 511
et al., 2021). 512

An evident limitation regarding the implemented muscle control scheme is worth high- 513
lighting. The effects of the coupled activation of the five intrinsic muscles on the glottal 514
posture and vocal fold configuration are simulated by applying the biomechanical model by 515
Titze and Hunter (2007) at a low-to-moderate computational cost. However, this model is 516
built around the effective displacement and rotation of the laryngeal cartilages on a trans- 517
verse glottal plane, and is not thus able to describe in full detail the 3D glottal adjustment, 518
in contrast with, for example, the anatomically accurate finite element models. Current 519
evidence supports that the arytenoid movement relative to an axis located at the CAJ and 520
perpendicular to the transverse glottal plane (see Figure 1(a)) is highly constrained, and 521
that a rocking-sliding motion about the long axis of the cricoid cartilage is more accurate 522
(Geng *et al.*, 2020; Yin and Zhang, 2014). The latter can explain in part the differences in 523
the simulated vocal fold posturing discussed in section III A, and it is expected to also affect 524
the three way coupling between tissue, airflow, and sound at the glottis. Furthermore, the 525
2D scheme neglects the changes in the medial surface shape and the vertical height of the 526
superior edge of the vocal folds (Movahhedi *et al.*, 2021), and underestimates the anatomical 527
constraints with extrinsic structures which can play a role during phonation (Moisik and 528
Gick, 2017). 529

Two important aspects regarding the biomechanical modeling of the laryngeal tissues 530
for the modified Kelvin model are highlighted. First, model parameters selection is key for 531

producing reliable responses. Although a number of references report biomechanical pa- 532
rameters for the main laryngeal tissues in humans (Hunter and Titze, 2007; Hunter *et al.*, 533
2004; Palaparthi *et al.*, 2019; Titze, 2006), the significant variability among the different 534
reported values is striking. The lack of consistent human data required a compromise that 535
considered laryngeal function in both animals and humans for the model. Thus, the ad 536
hoc values reported in Table IV correspond to those tissue parameters that yield the best 537
performance simultaneously for both the laryngeal posture model and the TBCM; notwith- 538
standing, significant differences with prior works are obtained, as evidenced in the simulated 539
muscle activation plots with vocal process distance and fundamental frequency. In addition, 540
each laryngeal tissue was modeled as a single one-dimensional fiber. This is a limitation to 541
accurately capture the distributed portions of the intrinsic muscles, especially for the thy- 542
rovocalis and thyromuscularis portions of the TA muscle. This could be extended by adding 543
independent submodels representing the different muscle portions, at the expense of increas- 544
ing the model complexity. We opted to keep the model with the single one-dimensional fiber 545
assumption for simplicity. 546

Note that the proposed scheme for the TBCM model continues to be an approximation 547
and has limitations that could be addressed in future studies, such as constraints for cartilage 548
displacements (Geng *et al.*, 2020; Hunter *et al.*, 2004), superior-inferior accommodation of 549
the larynx during phonation (Moisik and Gick, 2017), medial bulging, and anterior-posterior 550
gradient, among others. 551

Further assessment using heuristic or random control rules could provide additional in- 552
sights into the muscle control of the laryngeal function to disentangle the relations between 553

laryngeal function and the resulting acoustic output. Other future avenues for exploration 554
include the connection with a neurophysiological muscle activation that incorporates natural 555
neurological fluctuations in the activation of intrinsic laryngeal muscles (Manriquez *et al.*, 556
2019), and simulations of /VCV/ gestures to compute relative fundamental frequency. 557

V. CONCLUSIONS 558

A physiological scheme for controlling the mechanical properties of a triangular body 559
cover model of the vocal folds through the independent activation of the five intrinsic la- 560
ryngeal muscles is proposed. The approach builds upon prior efforts that describe rules 561
for controlling low-order models, vocal fold posturing, and a triangular vocal fold model. 562
The scheme provides a flexible and physiologically relevant way to control the self-sustained 563
fully interactive voice production model for both sustained vowels and time-varying glottal 564
gestures. At the same time, the resulting model allows for exploring the role of antagonistic 565
muscle pairs in phonation. The model simulations are in agreement with prior studies using 566
excised larynx experiments and high-order simulations. Using the proposed approach, we 567
illustrate that different states of activation can lead to the same vocal fold posturing, albeit 568
with highly different stress states. These similar posturing scenarios, however, have clear 569
differences in the resulting kinematic, aerodynamic, and acoustic measures of vocal func- 570
tion. The resulting model is a relevant tool that can provide key insights into the physical 571
mechanisms underlying normal and disordered phonation. 572

ACKNOWLEDGMENTS

573

This work was supported by ANID grants FONDECYT 1191369 and BASAL FB0008, 574
 STIC AmSud ASPMLM-Voice 21-STIC-05, and the National Institute on Deafness and 575
 Other Communication Disorders of the National Institutes of Health under award number 576
 P50DC015446. The content is solely the responsibility of the authors and does not neces- 577
 sarily represent the official views of the National Institutes of Health. 578

APPENDIX A:

579

The modified Kelvin model applied for simulating the laryngeal tissue is briefly described. 580
 It is a one-dimensional, biomechanical model for the internal stress-strain response in fibrous 581
 tissue given by Equation (A1). The main simulated variables are the axial stress, σ_i , and 582
 the axial strain, ϵ_i , for each tissue $i \in \mathcal{I}$. Equation (A1a) represents the total (passive plus 583
 active) stress, whereas Equation (A1b) describes active stress due to the internal contractile 584
 properties in the intrinsic muscles. 585

$$t_s \dot{\sigma}_i + \sigma_i = [\sigma_{a_i} + \sigma_{p_i} + Et_p \dot{\epsilon}_i], \quad (\text{A1a})$$

$$t_a \dot{\sigma}_{a_i} + \sigma_{a_i} = a_i \sigma_m \max \{0, 1 - b(\epsilon_i - \epsilon_m)^2\}, \quad (\text{A1b})$$

where a dot over a variable indicates time derivative, σ_{a_i} is the active stress, and σ_{p_i} is 586
 the passive viscoelastic stress corresponding to the fiber deformation ϵ_i modeled as follows 587

(Hunter *et al.*, 2004; Titze, 2006):

588

$$\begin{aligned}\sigma_{pi} &= -\frac{\sigma_0}{\epsilon_1}(\epsilon_i - \epsilon_1), & \epsilon_i \leq \epsilon_2, \\ &= -\frac{\sigma_0}{\epsilon_1}(\epsilon_i - \epsilon_1) + \sigma_2 [e^{B(\epsilon_i - \epsilon_2)} - 1 - B(\epsilon_i - \epsilon_2)], & \epsilon_i > \epsilon_2.\end{aligned}\tag{A2}$$

For non-contractile tissue (i.e., vocal ligament and mucosa) the active component is set to

589

zero.

590

Tissue-specific dynamical properties and stress-strain response characteristics in the Kelvin model of Equation (A1) can be specified independently by its parameters (Hunter *et al.*, 2004; Titze, 2006): t_s is a time-series constant, t_p is a parallel time constant, t_a is the internal activation time constant, A_i is the cross-sectional area, σ_m is the maximum isometric active stress, ϵ_m is the strain at maximum contractile stress, b is a coefficient for active stress, σ_0 is the stress at zero strain, σ_2 is a scale factor for the exponential function, B is an exponential strain constant, ϵ_1 is the strain at zero stress, and ϵ_2 is the strain at which the nonlinear exponential function begins. Moreover, $E = \frac{d\sigma_{pi}}{d\epsilon_i}$ is the nonlinear tangent Young's modulus. The resulting fiber force magnitude is $F_i = A_i\sigma_i$, where the force direction coincides with the longitudinal axis in the fiber. The parameters set in this work for modeling laryngeal tissue are reported in Table IV, whereas the remaining parameters are set as originally introduced in (Titze, 2006).

603

Alzamendi, G. A., Manríquez, R., Hadwin, P. J., Deng, J. J., Peterson, S. D., Erath,

604

B. D., Mehta, D. D., Hillman, R. E., and Zañartu, M. (2020). “ Bayesian estimation

605

of vocal function measures using laryngeal high-speed videoendoscopy and glottal airflow

606

- estimates: An in vivo case study ,” *The Journal of the Acoustical Society of America* 607
147(5), EL434–EL439, <http://asa.scitation.org/doi/10.1121/10.0001276>, doi: 10. 608
[1121/10.0001276](http://asa.scitation.org/doi/10.1121/10.0001276). 609
- Birkholz, P., Kröger, B. J., and Neuschaefer-Rube, C. (2011a). “Articulatory synthesis of 610
words in six voice qualities using a modified two-mass model of the vocal folds,” in *First* 611
International Workshop on Performative Speech and Singing Synthesis, Vancouver, British 612
Columbia, Canada. 613
- Birkholz, P., Kröger, B. J., and Neuschaefer-Rube, C. (2011b). “Synthesis of breathy, nor- 614
mal, and pressed phonation using a two-mass model with a triangular glottis,” in *Inter-* 615
speech 2011: 12th Annual Conference of the International Speech Communi- 616
cation Association, pp. 2681–2684, Florence, Italy. 617
- Chhetri, D. K., Neubauer, J., and Berry, D. A. (2012). “Neuromuscular control of funda- 618
mental frequency and glottal posture at phonation onset,” *The Journal of the Acousti-* 619
cal Society of America **131**(2), 1401–1412, [http://asa.scitation.org/doi/10.1121/1.](http://asa.scitation.org/doi/10.1121/1.3672686) 620
[3672686](http://asa.scitation.org/doi/10.1121/1.3672686), doi: 10.1121/1.3672686. 621
- Chhetri, D. K., Neubauer, J., Sofer, E., and Berry, D. A. (2014). “Influence and interactions 622
of laryngeal adductors and cricothyroid muscles on fundamental frequency and glottal 623
posture control,” *The Journal of the Acoustical Society of America* **135**(4), 2052–2064, 624
<http://asa.scitation.org/doi/10.1121/1.4865918>, doi: 10.1121/1.4865918. 625
- Cortés, J. P., Espinoza, V. M., Ghassemi, M., Mehta, D. D., Van Stan, J. H., Hillman, R. E., 626
Guttag, J. V., and Zañartu, M. (2018). “Ambulatory assessment of phonotraumatic vocal 627
hyperfunction using glottal airflow measures estimated from neck-surface acceleration,” 628

- PLOS ONE **13**(12), 1–22, <https://doi.org/10.1371/journal.pone.0209017>, doi: 10.1371/journal.pone.0209017. 629 630
- Erath, B. D., Zañartu, M., Stewart, K. C., Plesniak, M. W., Sommer, D. E., and Peterson, S. D. (2013). “A review of lumped-element models of voiced speech,” *Speech Communication* **55**(5), 667–690, doi: 10.1016/j.specom.2013.02.002. 631 632 633
- Espinoza, V. M., Mehta, D. D., Stan, J. H. V., Hillman, R. E., and Zañartu, M. (2020). “Glottal aerodynamics estimated from neck-surface vibration in women with phonotraumatic and nonphonotraumatic vocal hyperfunction,” *Journal of Speech, Language, and Hearing Research* **63**(9), 2861–2869, doi: 10.1044/2020_JSLHR-20-00189. 634 635 636 637
- Espinoza, V. M., Zañartu, M., Stan, J. H. V., Mehta, D. D., and Hillman, R. E. (2017). “Glottal aerodynamic measures in women with phonotraumatic and nonphonotraumatic vocal hyperfunction,” *Journal of Speech, Language, and Hearing Research* **60**(8), 2159–2169, doi: 10.1044/2017_JSLHR-S-16-0337. 638 639 640 641
- Farley, G. R. (1996). “A biomechanical laryngeal model of voice F₀ and glottal width control,” *The Journal of the Acoustical Society of America* **100**(6), 3794–3812, <http://asa.scitation.org/doi/10.1121/1.417218>, doi: 10.1121/1.417218. 642 643 644
- Galindo, G. E., Peterson, S. D., Erath, B. D., Castro, C., Hillman, R. E., and Zañartu, M. (2017). “Modeling the Pathophysiology of Phonotraumatic Vocal Hyperfunction With a Triangular Glottal Model of the Vocal Folds,” *Journal of Speech Language and Hearing Research* **60**(9), 2452–2471, http://jslhr.pubs.asha.org/article.aspx?doi=10.1044/2017_JSLHR-S-16-0412, doi: 10.1044/2017_JSLHR-S-16-0412. 645 646 647 648 649

- Geng, B., Pham, N., Xue, Q., and Zheng, X. (2020). “A three-dimensional vocal fold posturing model based on muscle mechanics and magnetic resonance imaging of a canine larynx,” *The Journal of the Acoustical Society of America* **147**(4), 2597–2608, <http://asa.scitation.org/doi/10.1121/10.0001093>, doi: 10.1121/10.0001093.
- Gömmel, A., Butenweg, C., Bolender, K., and Grunendahl, A. (2007). “A muscle controlled finite-element model of laryngeal abduction and adduction,” *Computer Methods in Biomechanics and Biomedical Engineering* **10**(5), 377–388, <https://www.tandfonline.com/doi/abs/10.1080/10255840701550923>, doi: 10.1080/10255840701550923.
- Hillman, R. E., Stepp, C. E., Van Stan, J. H., Zañartu, M., and Mehta, D. D. (2020). “An Updated Theoretical Framework for Vocal Hyperfunction,” *American Journal of Speech-Language Pathology* **29**(4), 2254–2260, doi: 10.1044/2020_AJSLP-20-00104.
- Huber, J. E., Stathopoulos, E. T., and Sussman, J. E. (2004). “The control of aerodynamics, acoustics, and perceptual characteristics during speech production,” *The Journal of the Acoustical Society of America* **116**(4), 2345–2353, <http://asa.scitation.org/doi/10.1121/1.1785571>, doi: 10.1121/1.1785571.
- Hunter, E. J., and Titze, I. R. (2007). “Refinements in modeling the passive properties of laryngeal soft tissue,” *Journal of Applied Physiology* **103**(1), 206–219, doi: 10.1152/japplphysiol.00892.2006.
- Hunter, E. J., Titze, I. R., and Alipour, F. (2004). “A three-dimensional model of vocal fold abduction/adduction,” *The Journal of the Acoustical Society of America* **115**(4), 1747–1759, <http://asa.scitation.org/doi/10.1121/1.1652033>, doi: 10.1121/1.1652033.

- Ibarra, E. J., Parra, J. A., Alzamendi, G. A., Cortés, J. P., Espinoza, V. M., Mehta, D. D., Hillman, R. E., and Zañartu, M. (2021). “Estimation of subglottal pressure, vocal fold collision pressure, and intrinsic laryngeal muscle activation from neck-surface vibration using a neural network framework and a voice production model,” *Frontiers in Physiology* **12**, 1419, <https://www.frontiersin.org/article/10.3389/fphys.2021.732244>, doi: [10.3389/fphys.2021.732244](https://doi.org/10.3389/fphys.2021.732244).
- Lester, R. A., Daliri, A., Enos, N., Abur, D., Lupiani, A. A., Letcher, S., and Stepp, C. E. (2020). “The relation of articulatory and vocal auditory & motor control in typical speakers,” *Journal of Speech, Language, and Hearing Research* **63**(11), 3628–3642, doi: [10.1044/2020_JSLHR-20-00192](https://doi.org/10.1044/2020_JSLHR-20-00192).
- Lowell, S. Y., and Story, B. H. (2006). “Simulated effects of cricothyroid and thyroarytenoid muscle activation on adult-male vocal fold vibration,” *The Journal of the Acoustical Society of America* **120**(1), 386–397, <http://asa.scitation.org/doi/10.1121/1.2204442>, doi: [10.1121/1.2204442](https://doi.org/10.1121/1.2204442).
- Lucero, J. C., and Schoentgen, J. (2015). “Smoothness of an equation for the glottal flow rate versus the glottal area,” *The Journal of the Acoustical Society of America* **137**(5), 2970–2973, <http://asa.scitation.org/doi/10.1121/1.4919297><http://dx.doi.org/10.1121/1.4919297>, doi: [10.1121/1.4919297](https://doi.org/10.1121/1.4919297).
- Manriquez, R., Peterson, S. D., Prado, P., Orio, P., Galindo, G. E., and Zanartu, M. (2019). “Neurophysiological Muscle Activation Scheme for Controlling Vocal Fold Models,” *IEEE Transactions on Neural Systems and Rehabilitation Engineering* **27**(5), 1043–1052, doi: [10.1109/TNSRE.2019.2906030](https://doi.org/10.1109/TNSRE.2019.2906030).

- Mehta, D. D., Espinoza, V. M., Van Stan, J. H., Zañartu, M., and Hillman, R. E. (2019). 693
“The difference between first and second harmonic amplitudes correlates between glottal 694
airflow and neck-surface accelerometer signals during phonation,” *The Journal of the* 695
Acoustical Society of America **145**(5), EL386–EL392, doi: [10.1121/1.5100909](https://doi.org/10.1121/1.5100909). 696
- Mehta, D. D., Van Stan, J. H., Zañartu, M., Ghassemi, M., Guttag, J. V., Espinoza, V. M., 697
Cortés, J. P., Cheyne, H. A., and Hillman, R. E. (2015). “Using ambulatory voice mon- 698
itoring to investigate common voice disorders: Research update,” *Frontiers in Bioengi-* 699
neering and Biotechnology **3**, 155, [https://www.frontiersin.org/article/10.3389/](https://www.frontiersin.org/article/10.3389/fbioe.2015.00155) 700
[fbioe.2015.00155](https://www.frontiersin.org/article/10.3389/fbioe.2015.00155), doi: [10.3389/fbioe.2015.00155](https://doi.org/10.3389/fbioe.2015.00155). 701
- Moisik, S. R., and Gick, B. (2017). “The Quantal Larynx: The Stable Regions of La- 702
ryngeal Biomechanics and Implications for Speech Production,” *Journal of Speech, Lan-* 703
guage, and Hearing Research **60**(3), 540–560, [http://pubs.asha.org/doi/10.1044/](http://pubs.asha.org/doi/10.1044/2016_JSLHR-S-16-0019) 704
[2016_JSLHR-S-16-0019](http://pubs.asha.org/doi/10.1044/2016_JSLHR-S-16-0019), doi: [10.1044/2016_JSLHR-S-16-0019](https://doi.org/10.1044/2016_JSLHR-S-16-0019). 705
- Movahhedi, M., Geng, B., Xue, Q., and Zheng, X. (2021). “Effects of cricothyroid and 706
thyroarytenoid interaction on voice control: Muscle activity, vocal fold biomechanics, flow, 707
and acoustics,” *The Journal of the Acoustical Society of America* **150**(1), 29–42, [https:](https://doi.org/10.1121/10.0005275) 708
[//doi.org/10.1121/10.0005275](https://doi.org/10.1121/10.0005275), doi: [10.1121/10.0005275](https://doi.org/10.1121/10.0005275). 709
- Palaparthi, A., Smith, S., and Titze, I. R. (2019). “Mapping Thyroarytenoid and Cricothy- 710
roid Activations to Postural and Acoustic Features in a Fiber-Gel Model of the Vocal 711
Folds,” *Applied Sciences* **9**(21), 4671, <https://www.mdpi.com/2076-3417/9/21/4671>, 712
doi: [10.3390/app9214671](https://doi.org/10.3390/app9214671). 713

- Poletto, C. J., Verdun, L. P., Strominger, R., and Ludlow, C. L. (2004). “Correspondence between laryngeal vocal fold movement and muscle activity during speech and nonspeech gestures,” *Journal of Applied Physiology* **97**(3), 858–866, <https://www.physiology.org/doi/10.1152/jappphysiol.00087.2004>, doi: 10.1152/jappphysiol.00087.2004.
- Story, B. H. (2008). “Comparison of magnetic resonance imaging-based vocal tract area functions obtained from the same speaker in 1994 and 2002,” *Journal of the acoustical society of America* **123**(1), 327–335, doi: 10.1121/1.2805683.
- Story, B. H., and Titze, I. R. (1995). “Voice simulation with a body-cover model of the vocal folds,” *The Journal of the Acoustical Society of America* **97**(2), 1249–1260, <http://asa.scitation.org/doi/10.1121/1.412234>, doi: 10.1121/1.412234.
- Titze, I. R. (2002). “Regulating glottal airflow in phonation: Application of the maximum power transfer theorem to a low dimensional phonation model,” *The Journal of the Acoustical Society of America* **111**(1), 367–376, <http://asa.scitation.org/doi/10.1121/1.1417526>, doi: 10.1121/1.1417526.
- Titze, I. R. (2006). *The Myoelastic Aerodynamic Theory of Phonation*, 1st edition ed. (National Center for Voice and Speech), <http://www.amazon.com/The-Myoelastic-Aerodynamic-Theory-Phonation/dp/0874141567>.
- Titze, I. R., and Hunter, E. J. (2007). “A two-dimensional biomechanical model of vocal fold posturing,” *The Journal of the Acoustical Society of America* **121**(4), 2254–2260, <http://asa.scitation.org/doi/10.1121/1.2697573>, doi: 10.1121/1.2697573.
- Titze, I. R., and Palaparthi, A. (2016). “Sensitivity of Source-Filter Interaction to Specific Vocal Tract Shapes,” *IEEE/ACM Transactions on Audio, Speech, and Language*

- Processing **24**(12), 2507–2515, <http://ieeexplore.ieee.org/document/7588050/>, doi: 736
[10.1109/TASLP.2016.2616543](https://doi.org/10.1109/TASLP.2016.2616543). 737
- Titze, I. R., Story, B., Smith, M., and Long, R. (2002). “A reflex resonance model of 738
vocal vibrato,” *The Journal of the Acoustical Society of America* **111**(5), 2272, [http://](http://scitation.aip.org/content/asa/journal/jasa/111/5/10.1121/1.1434945) 739
scitation.aip.org/content/asa/journal/jasa/111/5/10.1121/1.1434945, doi: 10. 740
[1121/1.1434945](https://doi.org/10.1121/1.1434945). 741
- Titze, I. R., and Story, B. H. (2002). “Rules for controlling low-dimensional vocal fold 742
models with muscle activation,” *The Journal of the Acoustical Society of America* **112**(3 Pt 743
1), 1064, <http://www.ncbi.nlm.nih.gov/pubmed/12243155>, doi: 10.1121/1.1496080. 744
- Van Stan, J. H., Ortiz, A. J., Cortés, J. P., Marks, K. L., Toles, L. E., Mehta, 745
D. D., Burns, J. A., Hron, T., Stadelman-Cohen, T., Krusemark, C., Muise, J., Fox- 746
Galalis, A. B., Nudelman, C., Zeitels, S., and Hillman, R. E. (2021). “Differences in 747
daily voice use measures between female patients with nonphonotraumatic vocal hyper- 748
function and matched controls,” *Journal of Speech, Language, and Hearing Research* 749
64(5), 1457–1470, https://pubs.asha.org/doi/abs/10.1044/2021_JSLHR-20-00538, 750
doi: [10.1044/2021_JSLHR-20-00538](https://doi.org/10.1044/2021_JSLHR-20-00538). 751
- Yin, J., and Zhang, Z. (2014). “Interaction Between the Thyroarytenoid and Lateral 752
Cricoarytenoid Muscles in the Control of Vocal Fold Adduction and Eigenfrequencies,” 753
doi: [10.1115/1.4028428](https://doi.org/10.1115/1.4028428). 754
- Zañartu, M. (2006). “Influence of acoustic loading on the flow-induced oscillations of single 755
mass models of the human larynx,” Master’s thesis, School of Electrical and Computer 756
Engineering, Purdue University, West Lafayette, IN. 757

- Zañartu, M., Galindo, G. E., Erath, B. D., Peterson, S. D., Wodicka, G. R., and Hillman, 758
R. E. (2014). “Modeling the effects of a posterior glottal opening on vocal fold dynam- 759
ics with implications for vocal hyperfunction,” The Journal of the Acoustical Society of 760
America **136**(6), 3262–3271, <http://asa.scitation.org/doi/10.1121/1.4901714>, doi: 761
[10.1121/1.4901714](http://dx.doi.org/10.1121/1.4901714). 762
- Zhang, Z. (2016). “Mechanics of human voice production and control,” The Journal of the 763
Acoustical Society of America **140**(4), 2614–2635, [http://asa.scitation.org/doi/10.](http://asa.scitation.org/doi/10.1121/1.4964509) 764
[1121/1.4964509](http://dx.doi.org/10.1121/1.4964509), doi: [10.1121/1.4964509](http://dx.doi.org/10.1121/1.4964509). 765

TABLE I. Anatomical and biomechanical parameters required for implementing the dynamic simulation of the laryngeal posturing and glottis configuration.

	Definition	Value
	Mass and moment of inertia	$M_{ac} = 1.4 \times 10^{-3}$ kg, $I_{ac} = 1.6 \times 10^{-6}$ kg m ² .
CAJ	Vocal process cadaveric position	$\bar{x}_0 = 4$ mm, $\bar{y}_0 = 0$ mm.
	CAJ center coordinates	$x_{CAJ} = 10.1$ mm, $y_{CAJ} = -10.1$ mm.
	Translational/rotational dampings	$d_x = 0.02$ s, $d_y = 0.02$ s, $\delta = 0.02$ s.
	Mass and moment of inertia	$M_{cc} = 10^{-2}$ kg, $I_{cc} = 10^{-5}$ kg m ² .
CTJ	CT/TA moment arms	$r_{TA} = 16.1$ mm, $r_{CT} = 11.1$ mm.
	CT angle relative to TA	$\phi = 45^\circ$, $\cos \phi = 0.76$.
	Translational/rotational viscous times	$t_t = 0.04$ s, $t_r = 0.04$ s.
Glottis	Rest VF length	$L_0 = 16$ mm.
	Posterior wall half-width coordinates	$x_{p2} = 3.2$ mm, $y_p = -2.5$ mm.

TABLE II. Three sets of appreciable different intrinsic muscle activation levels producing nearly the same simulated vocal process configurations.

Set	a_{LCA}	a_{IA}	a_{PCA}	a_{CT}	a_{TA}
\mathbf{a}_I	0.50	0.50	0.00	0.10	0.25
\mathbf{a}_{II}	0.40	0.40	0.00	0.15	0.40
\mathbf{a}_{III}	0.80	0.80	0.20	0.25	0.60

TABLE III. Effects of three different activation conditions on sustained phonation. Reported prephonatory posture parameters were obtained from the biomechanical larynx model. Kinematic, aerodynamic, and acoustic mean (SD) parameters were computed from simulated phonatory data considering tract area functions for vowels [æ ʌ ɑ e ε i o u υ] and driving pressure $P_s = 800$ Pa.

		Activation sets		
		\mathbf{a}_I	\mathbf{a}_{II}	\mathbf{a}_{III}
Posture	Strain ϵ [%]	-9.5	-11.3	-10.3
	VP Distance [%]	5.3	6.0	6.3
	A_{MGO} [mm ²]	0.8	0.9	1.0
	A_{PGO} [mm ²]	1.4	3.0	1.1
Kinematic	f_0 [Hz]	116.4 (4.7)	105.1 (4.4)	115.1 (3.7)
	OQ [%]	81.7 (7.6)	98.6 (3.8)	79.7 (11.7)
	CIQ [%]	24.0 (8.5)	33.9 (5.9)	25.5 (8.4)
Aerodynamic	AC Flow [mL/s]	395.2 (34.1)	367.6 (35.0)	372.2 (28.1)
	DC Flow [mL/s]	11.1 (1.1)	65.6 (1.7)	6.1 (1.0)
	MFDR [L/s ²]	710.6 (146.9)	375.7 (92.7)	648.4 (133.2)
	H1-H2 [dB]	12.9 (1.5)	12.7 (1.1)	12.2 (1.4)
Acoustic	SPL [dB]	84.9 (3.5)	77.2 (3.5)	84.5 (3.4)
	L/H Ratio [dB]	31.0 (14.1)	41.4 (4.7)	31.7 (14.1)

TABLE IV. Parameters for simulating laryngeal tissues according to the modified Kelvin model. Passive stress-strain response and active stress for the five intrinsic laryngeal muscles -CT: cricothyroid, TA: thyroarytenoid, LCA: lateral cricoarytenoid, IA: interarytenoid, and PCA: posterior cricoarytenoid-, the vocal ligament (LIG) and mucosa (MUC) are considered.

Parameter	Laryngeal muscles and tissues						
	CT	LCA	TA	IA	PCA	LIG	MUC
σ_0 [kPa]	2.2	3.0	2.0	2.0	5.0	2.0	1.0
σ_2 [kPa]	5.0	59.0	1.5	30.0	55.0	1.4	20.0
B [-]	7.0	4.0	6.5	3.5	5.3	13.0	4.4
ϵ_1 [-]	-0.5	-0.5	-0.5	-0.5	-0.5	-0.5	-0.5
ϵ_2 [-]	-0.06	-0.06	-0.05	-0.06	-0.05	-0.3	-0.3
σ_m [kPa]	300	100	150	100	100	—	—
ϵ_m [-]	0.0	0.4	0.2	0.4	0.4	—	—

List of Figures

766

1	(Color online) Main laryngeal structures involved in the prephonatory posturing. (a) Cricothyroid accommodation at the glottal plane; and (b) Projection of effective cricothyroid accommodation on the glottal plane. Glottal geometry and vocal fold adjustment are controlled via the relative accommodation of major laryngeal cartilages. Figures adapted from Titze (2006) . CAJ: cricoarytenoid joint, CTJ: cricothyroid joint.	767 768 769 770 771 772
2	(Color online) Schematic of the triangular body-cover model of the vocal folds.	11 773
3	(Color online) Simulated accommodation of the (right) arytenoid cartilage obtained by the independent activation of the five intrinsic muscles and the adductory complex. <i>Top</i> : Cartesian displacement of the cricoarytenoid joint (CAJ) center, $(x_{CAJ}+\xi, y_{CAJ}+\psi)$, and the vocal process (VP), (x_{02}, y_{02}) . The inset schematic illustrates the VP movements resulting from the displacement and rotation of the CAJ. <i>Bottom</i> : Rotation angle θ for the CAJ. Concurrent beginning of the paths indicates zero muscle activation.	774 775 776 777 778 779 18 780

4	<p>(Color online) Effects of laryngeal muscle coactivation on glottal adduction. 781</p> <p>Vocal process (VP) coordinates, (x_{02}, y_{02}), produced through the activation of 782</p> <p>the adductory complex for the non-coactivation case (solid line with medium 783</p> <p>markers), and for two activation levels for both TA muscle (dashed and dotted 784</p> <p>lines with small markers) and CT muscle (dashed and dotted lines with large 785</p> <p>markers). Three PCA activations are drawn in black ($a_{PCA} = 0.0$), dark color 786</p> <p>($a_{PCA} = 0.3$), and light color ($a_{PCA} = 0.6$) lines. Markers enclosed in circles 787</p> <p>indicate the results for null adductory complex activation ($a_{Add} = 0.0$). The 788</p> <p>inset schematic illustrates the VP Cartesian movements. 20 789</p>
5	<p>(Color online) Muscle activation plots for parametric coactivation of main 790</p> <p>phonatory intrinsic muscles. Vocal fold strain (left column) and vocal process 791</p> <p>distance (right column) are depicted as functions of the paired coactivation 792</p> <p>of muscle groups. The rows show four activation scenarios with contour lines 793</p> <p>included for clarity. For each row, A vs B refers to the abscissa and ordinate 794</p> <p>axes indicating activation levels for muscle groups A and B, respectively; null 795</p> <p>activations are set for the remaining intrinsic muscles. 21 796</p>

6	<p>(Color online) Muscle activation plots for parametric coactivation of adductory/abductory intrinsic muscles. Vocal fold strain (left column) and vocal process distance (right column) are depicted as functions of the paired coactivation of muscle groups. The rows show two activation scenarios with contour lines included for clarity. For each row, A vs B refers to the abscissa and ordinate axes indicating activation levels for muscle groups A and B, respectively; null activations are set for the remaining intrinsic muscles.</p>	<p>797 798 799 800 801 802 803</p>	23
7	<p>(Color online) Muscle activation plots with fundamental frequency for CT versus TA activation, considering different vocal tract shapes and subglottal pressures $P_s = [0.8, 1.4, 2.0]$ kPa. In all the cases $a_{LCA} = a_{IA} = 0.5$, and $a_{PCA} = 0.0$. The non-interactive case has no vocal tract and represents an excised larynx scenario. Isofrequency contours are drawn for clarity.</p>	<p>804 805 806 807 808</p>	26
8	<p>Simulated muscle control of voicing-devoicing for a /hi-hi-hi-hi/ gesture. From left to right, columns correspond to simulations for weak, moderate, and strong VF adduction with maximum activation levels 0.5, 0.6, and 0.7, respectively. Adductory signals a_{Add} are shown in the top row. The following three rows show the output signals for the glottal area A_g, glottal volume velocity U_g, and the radiated acoustic pressure P_o. The bottom row depicts the wideband spectrogram of P_o.</p>	<p>809 810 811 812 813 814 815</p>	28

9	Displacement paths for the right vocal process (VP), (x_{02}, y_{02}) , for three	816
	simulated tension states in the larynx. Trajectories correspond to laryngeal	817
	postures produced by parametric activation of the intrinsic muscles following	818
	the activation set $\mathbf{a} = [a_{LCA}, a_{IA}, a_{PCA}, a_{CT}, a_{TA}]$. The paths describe varia-	819
	tions for the normalized activations a_{Add} in the range of 0 to 1 in steps of 0.1.	820
	The inset schematic illustrates the VP Cartesian movements. Configurations	821
	enclosed in the dotted rectangle are considered for voiced sound simulations. 30	822